



Cite This: J. Phys. Chem. B 2019, 123, 3618-3629

pubs.acs.org/JPCB

Single Amino Acid Substitutions in Stickers, but Not Spacers, Substantially Alter UBQLN2 Phase Transitions and Dense Phase Material Properties

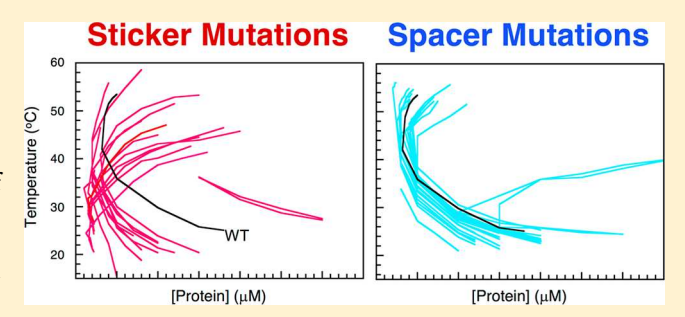
Published as part of The Journal of Physical Chemistry virtual special issue "Young Scientists".

Yiran Yang,[†] Holly B. Jones,^{‡,§} Thuy P. Dao,^{||} and Carlos A. Castañeda*,^{§,||}

[†]Department of Chemistry, [‡]Department of Biology, [§]Interdisciplinary Neuroscience Program, and ^{||}Departments of Biology and Chemistry, Syracuse University, Syracuse, New York, United States

Supporting Information

ABSTRACT: UBQLN2 450–624 oligomerizes and undergoes temperature-responsive liquid—liquid phase transitions following a closed-loop temperature—concentration phase diagram. We recently showed that disease-linked mutations to UBQLN2 450–624 impart highly varying effects to its phase behavior, ranging from little change to significant decrease of saturation concentration and formation of gels and aggregates. However, how single mutations lead to these properties is unknown. Here, we use UBQLN2 450–624 as a model system to study the sequence determinants of phase separation. We hypothesized that UBQLN2 450–624 regions



previously identified to promote its oligomerization are the "stickers" that drive interchain interactions and phase separation. We systematically investigated how phase behavior is affected by all 19 possible single amino acid substitutions at three sticker and two "spacer" (sequences separating stickers) positions. Overall, substitutions to stickers, but not spacers, substantially altered the shape of the phase diagram. Within the sticker regions, increasing hydrophobicity decreased saturation concentrations at low temperatures and enhanced oligomerization propensity and viscoelasticity of the dense phase. Conversely, substitutions to acidic residues at all positions greatly increased saturation concentrations. Our data demonstrate that single amino acid substitutions follow a molecular code to tune phase transition behavior of biopolymers.

■ INTRODUCTION

Liquid-Liquid phase separation (LLPS) is a process by which a solution of macromolecules demixes into a species-rich liquid dense phase in equilibrium with a species-poor dilute phase. LLPS is hypothesized to underlie the assembly of biomolecular condensates essential for various cellular processes. 1,2 In phaseseparating proteins, a major characteristic is multivalency, the existence of multiple associative motifs of intrinsically disordered segments or structured domains that form intraand interchain interactions.³⁻⁵ Accumulating evidence shows that phase transition behavior is encoded in the amino acid sequence.^{6–8} Mutations can tune the conditions necessary for LLPS, as well as the material properties of these condensates in vitro and in vivo. 9,10 Indeed, dysregulation of condensate dynamics, assembly, and/or disassembly is linked to diseases, including amyotrophic lateral sclerosis (ALS) among others. Therefore, deciphering the molecular code that drives phase transitions of biopolymers is key to understanding diseases, as well as designing stimuli-responsive polymers with emergent properties.

The "stickers" and "spacers" framework is emerging as useful language to describe the physical origins of LLPS behavior in proteins. Stickers are the associative motifs that drive LLPS,

whereas the spacers connect the sticker regions and tune LLPS behavior as well as impart flexibility. $^{11-13}$ The chemical basis of sticker interactions that govern phase transition behavior varies across phase-separating systems. For instance, Arg and Tyr residues in the FUS family of proteins use cation— π and π — π stacking interactions to drive LLPS. The hydrophobic effect modulates LLPS of elastin and elastin-like proteins and other proteins such as Pabl. LLPS. Aromatic residues are essential for mediating TDP-43 LLPS. Electrostatic interactions formed via clusters of either positively or negatively charged residues stabilize Ddx4 protein droplets. These experimental data must be combined to deduce the molecular grammar underpinning LLPS at physiological conditions for biological systems. Indeed, π — π contact propensity can be used to predict LLPS based solely on amino acid sequence.

Evaluating the effects of amino acid substitutions on phase transition behavior requires elucidation of full phase diagrams that map the conditions where the solution phase separates into protein-dilute and protein-dense phases. For some

Received: January 31, 2019 Revised: March 25, 2019 Published: March 29, 2019



systems, the protein-dense phase also intersects a liquid-gel phase boundary, where the dense phase undergoes gelation, a transition from liquid droplets to a noncovalent physically cross-linked network of molecules. 11 The equilibrium protein concentrations in the protein-dilute and protein-dense phases are described by the binodal or coexistence curve comprising both low and high concentration arms. The low concentration arm defines the protein saturation concentration (c_s) , below which the system will be mixed and homogeneous, and above which, the system will form a distinct second phase such as protein-dense liquid droplets. 20–22 Coexistence curves are determined by the free energy of the system thereby including entropy of mixing, as well as the enthalpies of protein-protein, protein-solvent, and solvent-solvent interactions. The complex interplay of these terms provides the thermodynamic basis for LLPS in biological systems. Obtaining experimental phase diagrams and predicting these via computational modeling and/or simulation are ideal metrics to determine the molecular driving forces of phase separation and phase separation-driven gelation. 11,23 Therefore, experimental systems are needed to address this goal, as emphasized in recent literature.^{22,7}

We established a model biopolymer system, the C-terminal construct of UBQLN2 (450-624), to which we could experimentally map the effects of single amino acid substitutions on phase transition behavior. We recently demonstrated that UBQLN2, a proteasomal shuttle factor involved in cellular protein quality control mechanisms, phase separates under physiological conditions, and that UBQLN2 450-624 generally mimics the LLPS behavior of full-length UBQLN2.25 Furthermore, UBQLN2 450-624 can be easily expressed and purified from bacteria, enabling the establishment of a large mutagenesis library to study the sequence effects on phase transitions. We previously identified regions of UBQLN2 450-624 important for oligomerization and hypothesized that these same segments are the stickers that drive LLPS. To test this hypothesis, we systematically substituted each of the natural amino acids into three sticker and two spacer positions and obtained low-concentration arms of temperature-concentration phase diagrams. In agreement with the stickers and spacers framework, only sticker substitutions substantially altered the shape of temperature concentration phase diagrams, whereas spacer substitutions only marginally affected coexistence curves. Increasing hydrophobicity of the amino acid substitution shifted coexistence curves such that UBQLN2 phase separated at lower temperatures and concentrations. Our data illustrate that single amino acid substitutions at designated positions in the amino acid sequence of a protein substantially modify phase transition behavior of biopolymers. These data can be used to benchmark analytical and computational models of phase transitions.

METHODS

Subcloning, Protein Expression, and Purification. UBQLN2 mutants were generated from UBQLN2 450–624 using Phusion Site-Directed Mutagenesis Kit (Thermo Scientific). A tryptophan codon was added to the C-terminal end of all constructs to facilitate determination of protein concentration (Figure S1A). UBQLN2 450–624 and all the mutants were expressed and purified as described by Dao et al, 2018. Briefly, the constructs were expressed in *Escherichia coli* Rosetta 2 (DE3) pLysS cells in Luria—Bertani (LB) broth at 37 °C overnight. Bacteria were pelleted, frozen, lysed, then purified via a "salting out" process. NaCl was added to the

cleared lysate to the final concentration of 0.5-1 M. UBQLN2 droplets were pelleted and then resuspended in 6 M urea, 20 mM sodium phosphate, 0.5 mM ethylenediaminetetraacetic acid (EDTA), 0.1 mM tris(2-carboxyethyl)phosphine (TCEP), 0.02% NaN₂ (pH 6.8). Leftover NaCl and urea were removed through HiTrap desalting column (GE Healthcare). All the cysteine mutants were subjected to size exclusion chromatography (SEC) over a Superdex 75 HiLoad 16/600 column (GE Healthcare) or an ENrich SEC 650 10 × 300 column (Biorad) to remove dimer contaminations. Sodium dodecyl sulfatepolyacrylamide gel electrophoresis (SDS-PAGE) gels were performed to confirm the purity of the proteins (Figure S2A). The identity and molecular weight of each mutant was verified using electrospray mass spectrometry in positive mode on a Shimadzu 8040 MS (Figure S2B). Purified proteins were frozen at -80 °C.

Spectrophotometric Absorbance/Turbidity Measurements. Protein samples were prepared by adding protein (from stock to a final concentration of 50 μ M unless otherwise noted) to cold sodium phosphate buffer (pH 6.8, 20 mM NaPhosphate, 0.5 mM EDTA, 0.1 mM TCEP, 0.02% NaN₃) containing 200 mM NaCl and were kept on ice for at least 5 min before the assay. Absorbance at 600 nm was recorded as a function of temperature by a Beckman DU-640 UV/vis spectrophotometer using a temperature ramp rate of 2 °C/min increasing from 16 to 60 °C and then ramped down to 16 °C. Net absorbance values were recorded after subtracting the absorbance value of a buffer control. Results were averaged from data collected using proteins from at least two separate preps and four trials for each (total $n \ge 8$) (Figure S2C). Data were plotted using Mathematica (Wolfram Research).

Phase Diagram Measurements. For the lower critical solution temperature (LCST) phase transition, that is, mapping the phase boundary as temperature is increased, protein samples were prepared as described for the turbidity measurements. For the upper critical solution temperature (UCST) arm, protein samples were prepared by mixing protein and buffer/salt solutions that were incubated at 63 °C for at least 10 min. Absorbance at 600 nm was recorded as a function of temperature by a Beckman DU-640 UV/vis spectrophotometer using a temperature ramp rate of 2 °C/ min decreasing from 60 to 16 °C. Two trials (n = 2) were conducted using four to five different concentrations of wildtype (WT) and mutant UBQLN2 450-624 proteins for each arm. The protein concentrations were chosen to cover as wide a range as possible to allow observation of phase separation during the temperature ramps but not at the starting temperatures (16 and 60 °C for LCST and UCST arms, respectively). Cloud-point temperatures were determined by fitting a Four Parameter Logistic Regression model to the data (Figure S3).

$$y = d + \frac{a - d}{1 + \left(\frac{x}{c}\right)^b} \tag{1}$$

Cloud-point temperatures used were the points of inflection (c). Cloud-point temperatures were then used to define the coexistence curve as a function of protein concentration. The temperature ramp rate was either 1 or 2 $^{\circ}$ C/min, whichever yielded the most reproducible, consistent turbidity profiles and phase diagrams. Specifically, a 1 $^{\circ}$ C/min ramp rate was used for the LCST arms of hydrophobic and aromatic substitutions.

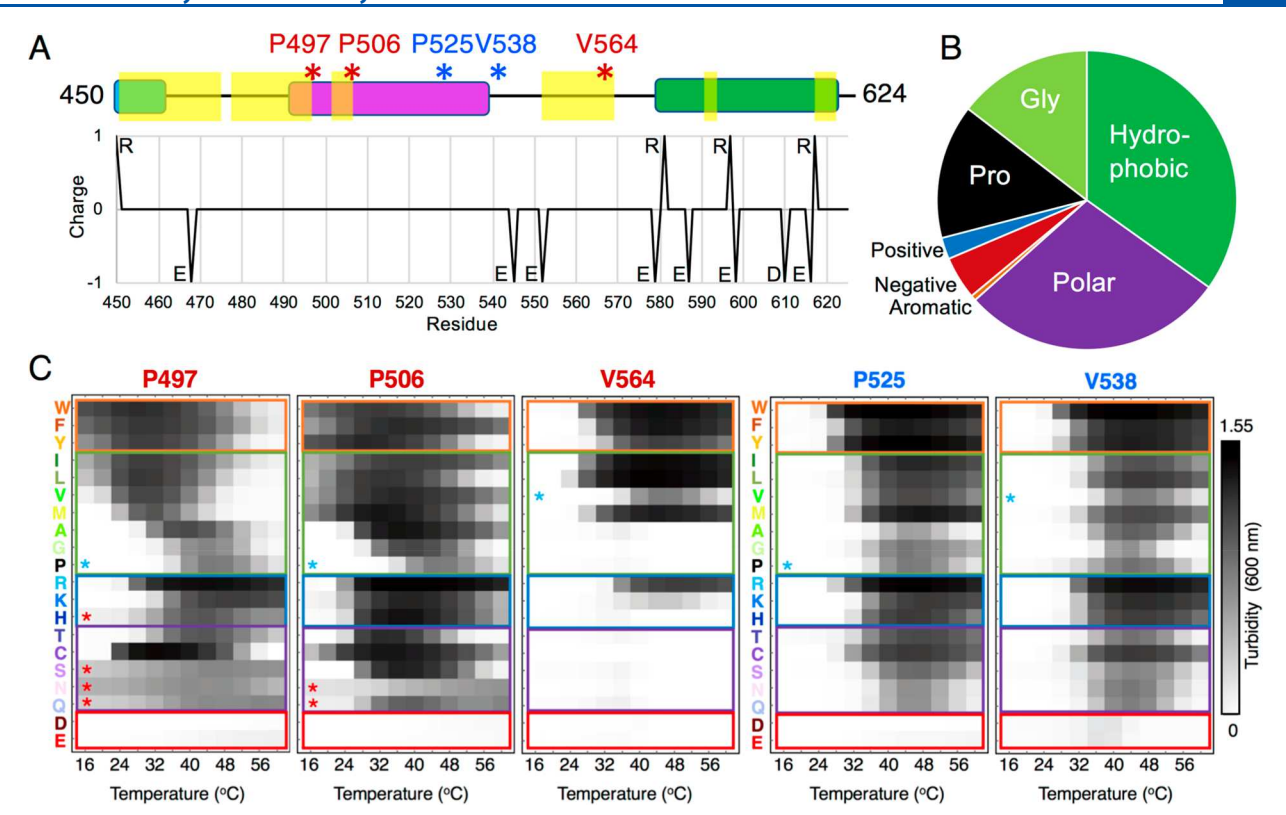


Figure 1. Turbidity assay screens for mutants in sticker and spacer regions of UBQLN2 450–624. (A) Domain architecture of UBQLN2 450–624 with STI1-II, PXX, and UBA domains colored as cyan, magenta, and green, respectively. Highlighted in yellow are regions identified by NMR to promote UBQLN2 oligomerization and hypothesized to be stickers. Red and blue labels represent sticker and spacer positions studied here, respectively. Immediately below marks the location of ionizable residues and their expected charge state at pH 7. All of the arginines and most of the negatively charged residues reside in the folded UBA domain. (B) Fraction of the different types of amino acids in UBQLN2 450–624, which is high in hydrophobic, polar, glycine, and proline and depleted of aromatic and charged residues. Pie chart follows the general organization in Ruff et al. 2018. (C) Results from spectrophotometric turbidity assay as a function of temperature comparing LLPS of different UBQLN2 mutants using 50 μM protein in 20 mM NaPhosphate and 200 mM NaCl (pH 6.8). The blue asterisks represent WT UBQLN2 turbidity profile for each position. The red asterisks represent mutants that form unevenly distributed aggregates at one point during the assay. P497H, S, N, and Q formed aggregates early in the experiment, whereas P506N and Q aggregated at temperatures above 44 °C. Turbidity profiles of amino acid substitutions at each position are separated by amino acid type: aromatic, hydrophobic, basic, polar, and acidic. Hypothesized stickers and spacers are color-coded red and blue, respectively, at the top.

Fitting and plotting of data were done with Kaleidagraph (Synergy Software).

Bright-Field Imaging of Phase Separation. UBQLN2 450–624 constructs were prepared to contain 100 μ M protein in 20 mM NaPhosphate, 200 mM NaCl, 0.1 mM TCEP, and 0.5 mM EDTA (pH 6.8). Samples were added to MatTek glass-bottom dishes that had been coated with 5% bovine serum albumin (BSA), to minimize changes as a result of surface interactions, and incubated at 37 °C. Phase separation was imaged on an ONI Nanoimager (Oxford Nanoimaging Ltd.) equipped with a Hamamatsu sCMOS ORCA flash 4.0 V3 camera using an Olympus 100 × /1.4 N.A. objective. Images were prepared using Fiji²⁶ and FigureJ plugin.²⁷

Droplet Fusion Assays. UBQLN2 450–624 constructs were prepared to contain 100 μ M protein in 20 mM NaPhosphate and 0.5 mM EDTA (pH 6.8), except for P506W at 25 μ M protein and P506E and V538E at 300 μ M protein. Samples were added to MatTek glass-bottom dishes that had been incubated with 5% BSA (to minimize changes as a result of surface interactions) and incubated at 37 °C. Phase separation was initiated with the addition of NaCl to a final concentration of 200 mM. After 10 min of incubation, droplet formation was imaged as time-lapsed sequences for 3 min on an ONI Nanoimager equipped with a Hamamatsu sCMOS

ORCA flash 4.0 V3 camera using an Olympus 100 × /1.4 N.A. objective. Five trials were performed for each mutant. Droplets chosen for analysis were of similar size and ranged between 2 and 4 μ m, except for V538E (8 μ m) and P506E (5 μ m). For each mutant, eight fusion events were chosen for analysis and saved as separate TIFF images including frames from the initial fusion event.

Relaxation times (time it takes for two fusing droplets to return to a round shape) were determined by manually measuring the major axis (a) and the minor axis (b) in pixels using Fiji software²⁶ and calculating the aspect ratio as $\alpha = a/b$. We monitored the fusion events in this way, until the droplets reached their most relaxed state, or until the aspect ratio was approximately equal to 1. The aspect ratio for each fusion event was fit to an exponential decay curve in Matlab (Mathworks).

$$y = (\alpha_0)e^{-x/\tau} + c \tag{2}$$

where α_0 is the initial aspect ratio, x is time, and τ gives the characteristic relaxation time.

Size Exclusion Chromatography. Purified UBQLN2 constructs at different concentrations (10, 100, and 500 μ M) were subjected to chromatography over an ENrich SEC 650 10

× 300 column (Biorad) on a Biorad NGC FPLC system. Experiments were conducted using 250 µL of protein at ambient temperature using 1 mL/min flow rate in pH 6.8 buffer containing 20 mM NaPhosphate, 0.5 mM EDTA, and 0.1 mM TCEP with no added NaCl.

RESULTS

Library Generation of UBQLN2 Mutants. We previously characterized the LLPS properties of full-length UBQLN2 and several deletion constructs, including UBQLN2 450-624.²⁵ We showed that UBQLN2 oligomerization is a prerequisite for UBQLN2's ability to phase separate in vivo and in vitro, as expected and observed for many other LLPS systems. For detailed biophysical analyses, we focused on UBQLN2 450-624 (Figure S1A), whose small size (~175 amino acids) enabled the use of nuclear magnetic resonance (NMR) spectroscopy to monitor backbone amide chemical shifts as a function of protein concentration on a residue-by-residue basis. We observed concentration-dependent chemical shifts for residues 450-509, 555-570, 592-596, and 615-620, indicating that these residues are involved in UBQLN2 oligomerization (Figures 1A and S1A,B). Here, we hypothesized that the residues in these segments comprise the sticker regions that drive UBQLN2 phase separation. The amino acid compositions of these sticker regions and of UBQLN2 450-624 are hydrophobic and polar (Figures 1B and S1A,C), consistent with other polymers that phase separate as temperatures increase such as elastin-like polypeptides (ELPs).¹⁵

We recently showed that ALS-linked mutations P497H, P497L, P497S, P506A, P506S, and P506T, but not P525S, significantly altered UBQLN2 450-624 LLPS properties.⁴³ Interestingly, on the basis of our NMR data, residues P497 and P506 are in a sticker region, and P525 is in a spacer region. We hypothesized that mutations in the sticker regions would greatly affect both the dense and dilute phases (e.g., saturation concentrations, droplet morphology, droplet fusion kinetics), whereas mutations in the spacer regions would not. To test this hypothesis, we sought to determine the effects of amino acid substitutions at these three positions as well as at an additional sticker position, V564, and spacer position, V538, in the UBQLN2 450-624 background, hereafter referred to as UBQLN2 (Figure 1A). All five positions reside in the intrinsically disordered segment between residues 450 and 580.²⁵ We generated all 19 possible amino acid substitutions at each of these positions for a total of 95 mutant constructs. We expressed and purified wild-type and mutant UBQLN2 proteins from E. coli. As done previously, we used salt-induced phase separation and centrifugation to separate UBQLN2 from the rest of the E. coli lysates and then desalted into non-phase separating pH 6.8 buffer containing 20 mM NaPhosphate. Proteins were more than 95% pure (Figure S2A).

Turbidity Assays Screened for Effects of Amino Acid Substitutions on LLPS. To systematically screen for the effects of UBQLN2 mutations on LLPS, we monitored the change of A_{600} values between 16 and 60 °C of samples containing a fixed protein concentration and buffer composition (see Methods). Previous work from our lab showed that high and low A_{600} values correlate with UBQLN2 droplet formation and droplet clearance, respectively.²⁵ To ensure reproducibility, we repeated these assays a minimum of eight times using at least two purified protein stocks (Figure S2C).

Wild-type UBQLN2 undergoes two temperature-responsive phase transitions (Figure 1C). First, UBQLN2 phase separates as temperature is increased between 16 and 45 °C. This phase transition has an LCST, below which the protein solution is always mixed, regardless of protein concentration. Second, a solution of phase-separated UBQLN2 becomes less turbid as temperature is increased between 45 and 60 °C. This second phase transition has a UCST, above which the protein solution is always mixed. Together, these data are indicative of phase behavior following a UCST + LCST closed-loop phase diagram (Figure 2A).²² Turbidity was generally reversible when temperature was decreased from 60 to 16 °C (Figure S2D). These results are consistent with our prior work.⁴³

Focusing first on the overall turbidity assay trends across all positions, we immediately noticed that mutations in sticker positions 497, 506, and 564 substantially impacted the temperature ranges where phase separation was observed, as compared to mutations in spacer positions 525 and 538. There is considerable variation in the extent of phase separation among the different amino acid substitutions in the sticker positions. It is important to note that, for positions 497, 506, and 525, the wild-type amino acid is proline, whereas for positions 538 and 564, it is valine. Regardless of the wild-type amino acid, the trends for spacer positions 525 and 538 were nearly identical. In contrast, the overall extent of phase separation for the sticker substitution at position 564 was greatly reduced compared to positions 497 and 506. The turbidity data across the five positions were consistent with our initial hypothesis that residues 497, 506, and 564 are stickers, whereas residues 525 and 538 are spacers (Figure 1C).

Second, we organized our turbidity assay results by amino acid type: hydrophobic (A, G, I, L, M, P, V), aromatic (F, W, Y), basic (H, K, R), acidic (D, E), and polar (C, N, Q, S, T). We note the difficulties in assigning amino acids to these classes, particularly G and P, due to their roles in modulating protein flexibility and solubility.²⁸ We presented our amino acid substitutions in terms of decreasing hydrophobicity, largely following the experimental hydrophobicity scale determined by Urry et al., 1992.²⁹ Among the sticker positions 497, 506, and 564, increased hydrophobicity promoted UBQLN2 LLPS and lowered the temperature threshold for phase separation. Aromatic substitutions at the sticker positions decreased the temperatures when phase separation was first observed, in many cases below 16 °C, the starting temperature of the experiment. Notably, the effects on the mutations on the turbidity profiles varied by position even among stickers. For example, UBQLN2 mutants with Ile or Phe substitutions at position 506 remained turbid for the entire temperature range (16-60 °C), whereas phase-separating solutions of P497F and P497I began clarifying at 40 °C. These observations illustrated that Ile and Phe substitutions to both P497 and P506 impact LCST and UCST phase transitions but via different mechanisms. Of the 95 mutants, only six visibly aggregated during the turbidity assay experiments: P497H, P497S, P497N, P497Q, P506N, and P506Q (Figure S2E). Of these, two are disease-linked mutations (P497H and P497S). Although the effects of the spacer mutations on LLPS were much less drastic compared to those in the sticker positions, we still observed large increases in the absolute intensity of the absorbance signal, especially among substitutions to aromatic and more hydrophobic residues. It is possible that these substitutions made the spacer positions more sticker-like, hence increasing the degree of phase separation of the solution.

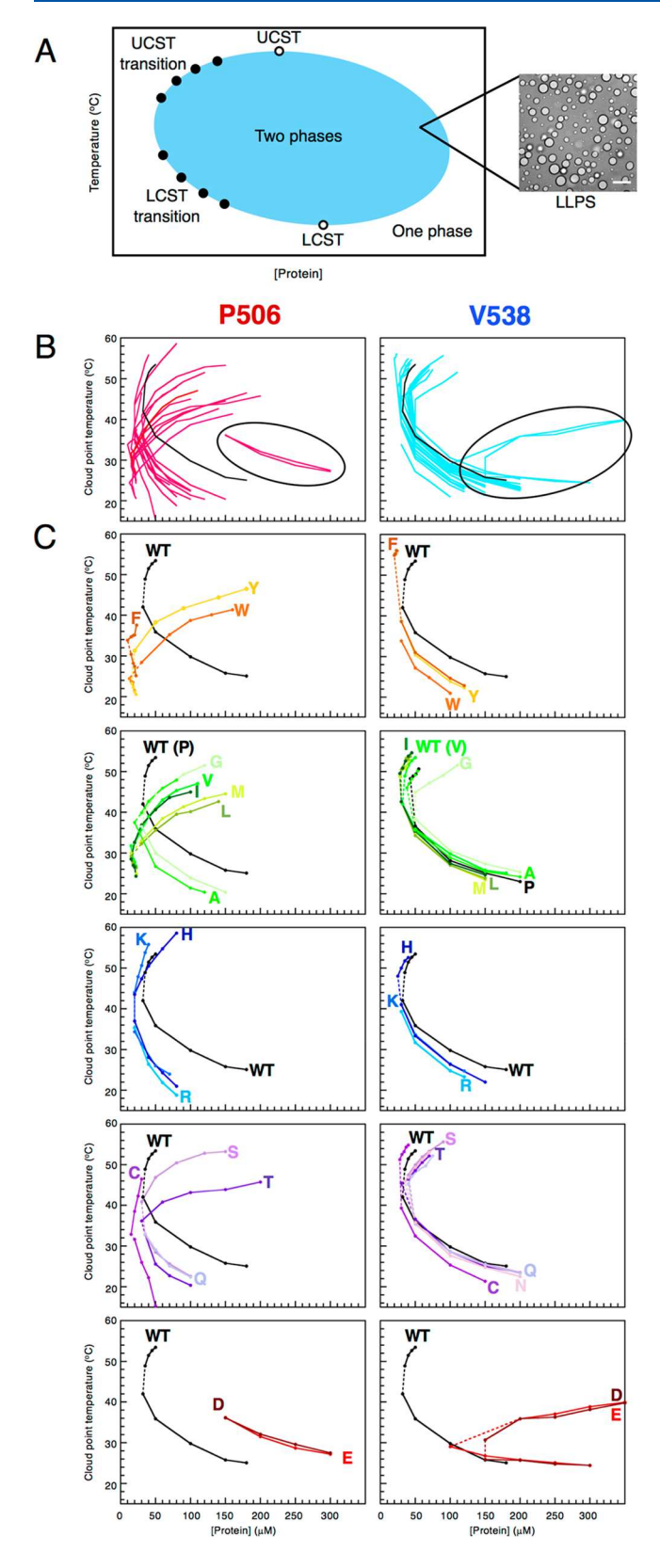


Figure 2. Temperature—Concentration phase diagrams for representative sticker and spacer residues in UBQLN2. (A) Schematic of a closed-loop phase diagram showing both UCST and LCST behaviors. The black dots represent the experimental data points for the low concentration arm obtained in this study to partially map the phase diagram. (B) Effects of amino acid substitutions in the sticker (pink, P506) region and in the spacer (cyan, V538) region compared to WT UBQLN2 (black). Circled in black are D and E mutants for each

Figure 2. continued

position. (C) Effects of amino acid substitutions separated by amino acid type: aromatic (F, W, Y), hydrophobic (A, G, I, L, M, P, V), basic (H, K, R), polar (C, N, Q, S, T), and acidic (D, E). The dashed lines are guides that connect the UCST phase transition cloud-point temperatures to the LCST ones. Both arms of P506N and the UCST arm of P506Q are missing due to formation of aggregates during the assays. The UCST arms for V538W, V538Y, V538R, V538K, P506D, and P506E are missing, since we observed either no turbidity or nonzero turbidity values at 60 °C at all concentrations tested.

Morever, the turbidity assay does not directly measure the number of droplets but the scattering of the samples. Scattering is highly dependent on differences in the size of the droplets, which might change as the result of the substitutions. One notable similarity between stickers and spacers was the effect of Asp and Glu substitutions, both of which significantly disrupted phase separation at all positions tested. Together, these data emphasize that perturbations to LLPS properties of proteins are very sensitive to both the type of amino acid substitution and the position in the amino acid sequence.

Effects of Amino Acid Substitutions on Phase Diagrams. To quantitatively compare the effects of single amino acid substitutions on phase transitions of UBQLN2 and determine the driving forces for UBQLN2 phase separation, we experimentally obtained temperature-concentration phase diagrams for the 19 substitutions at two representative positions: a sticker residue (P506) and a spacer residue (V538) (Figure 2). At a protein concentration for which no LLPS was observed at the start of the experiment, we performed temperature-ramping turbidity assays and determined $T_{cp}(infl)$, the cloud-point temperature at the inflection point of the transition (Figure S3).³⁰ There are other methods to characterize the conditions when phase transitions occur, including using microscopy to monitor onset or applying a threshold to changes in absorbance-temperature curves. For practical reasons, we chose the inflection point, $T_{cp}(infl)$, for comparison across different protein samples. The experimental $T_{\rm cp}$ values at different protein concentrations were used to map the coexistence curves (Figure 2). Since UBQLN2 exhibits both LCST and UCST phase transition behavior, $T_{\rm cp}$ associated with the LCST transition was determined by increasing temperature from 16 to 60 °C, whereas $T_{\rm cp}$ values associated with the UCST transition were determined by starting turbidity assay experiments at 60 °C and ramping down to 16 °C (see Methods). We tried these experiments at low (μM) as well as high (up to 3 mM) protein concentrations. However, the protein solutions were always cloudy or contained aggregates at the higher concentration ranges at the start of the experiments (both 16 and 60 °C). Therefore, we focused on obtaining the low-concentration arm (c_s) of the coexistence curves (Figure 2A). As expected from the turbidity assays (Figure 1C), the experimental phase diagram for WT UBQLN2 resembles that of a UCST-LCST closed-loop phase diagram, indicating two temperatureresponsive phase transitions between 16 and 60 °C (Figure 2B).

Strikingly, amino acid substitutions at sticker position 506 not only shifted the position of the coexistence curves but also changed the overall shape of the phase diagram (Figure 2B). Meanwhile, amino acid substitutions at spacer position 538

only mildly shifted coexistence curves but generally displayed a phase diagram with similar shape to that of WT. In other words, mutations at position 538 minimally perturbed the $c_{\rm s}$ needed for LLPS. These observations are entirely consistent with the expected behaviors of stickers and spacers. ^{8,20} The major exceptions to these observations were acidic amino acid substitutions, for which the $c_{\rm s}$ values of the dilute phase were greatly increased for all positions (see below).

Among the classes of amino acid substitutions, aromatic and hydrophobic amino acid mutations at sticker position 506 substantially affected the phase diagram of UBQLN2. Furthermore, increasing hydrophobicity of the amino acid substitution correlated with decreasing $c_{\rm s}$ values of the LCST phase transition. The coexistence curves all shifted to the left as hydrophobicity of the amino acid substitution increased. These data are completely consistent with our prior work that showed lowered $c_{\rm s}$ of UBQLN2 for hydrophobic disease-linked mutations T487I and P497L. Together, the data suggest the importance of the hydrophobic amino acids in driving UBQLN2 phase separation. Indeed, many of the amino acids in sticker regions are hydrophobic, as we previously characterized (Figure S1A).

At position 506, aromatic substitutions substantially changed the shape of UBQLN2's phase diagram, but differently depending on the amino acid. Tyr and Trp mutations shifted the UCST arm of the phase diagram downward compared to WT, with UCST cloud-point temperatures below 50 °C at least up to 200 µM protein concentrations. On the one hand, the Phe substitution was always phase separated over the entire temperature range tested, except at low protein concentrations ($<20 \mu M$). In contrast, the Phe substitution at position 538 minimally impacted the overall shape of the phase diagram, while all aromatic substitutions at this position imposed a leftward shift of the coexistence curves to lower protein concentrations. Notably, we could not obtain V538 Tyr and Trp UCST phase transition cloud points, since we could not establish clear baselines at 60 °C for any protein concentrations that exhibited turbidity during the temperature ramping assays. Therefore, these cloud-point values are likely to be greater than 60 °C. We speculate that the aromatic substitutions impart stickerlike properties to position 538, thus decreasing the c_s values for LLPS. It is apparent that π -stacking interactions involving aromatic amino acids promote LLPS in other systems, such as FUS and TDP-43.8,

Polar substitutions at the sticker but not spacer position affected the phase diagram of UBQLN2. This makes sense given the polar amino acid composition (Figure 1B). At position 506, both LCST and UCST transitions were perturbed. Interestingly, the LCST transitions of Ser, Thr, and Gln substitutions nearly superimposed, while the UCST arm of the coexistence curves decreased in the order C > S > T. We also noted that five of the six substitutions that produced aggregates (Figure S2E) were polar substitutions: P497S, P497Q, P497N, P506Q, P506N.

Basic amino acid substitutions shifted coexistence curves to the left, with little difference among the three basic amino acids (His, Lys, Arg). The effects were more substantial for the sticker position than for the spacer. Interestingly, acidic amino acid substitutions had the opposite effects and greatly increased the saturation concentrations needed for UBQLN2 LLPS, as well as narrowing the temperature region where the protein phase-separated. We speculate that these effects can be partially explained by the bulkiness of the side-chain

substitution (for Arg and Lys, whose side chains have some hydrophobic character) as well as the charge state of the UBQLN2 construct. At 25 °C, the predicted pI or isoelectric point of the UBQLN2 450–624 construct is ~4.4, with less than 7% of the protein containing ionizable residues (Figure 1B). This means that the protein is negatively charged at pH 6.8, the pH chosen for our experiments. Introduction of positive charges provides attractive Coulombic interactions between the substitution and the overall charge of the protein, thereby promoting intermolecular interactions between UBQLN2 molecules to drive phase separation. In contrast, acidic substitutions may do the opposite, potentially providing repulsive interactions between UBQLN2 molecules and decreasing phase separation.

Hydrophobic Sticker but Not Spacer Substitutions **Altered Droplet Morphology and Increased Viscoelastic** Properties. Mapping the lower concentration arms of the phase diagram allowed us to evaluate the effects of the substitutions on the dilute phase. However, what are the consequences of the substitutions on the dense phase? To answer this, we first used brightfield microscopy to investigate the morphology of UBQLN2 droplets of representative amino acid substitutions from the different classes of residues, including W (aromatic), G and L (hydrophobic), R (basic), Q (polar), and E (acidic) across the five positions studied here (Figure 3A). In general, the droplet morphologies at these different positions correlated well with the turbidity assay results. Mutants exhibiting similar turbidity profiles as WT UBQLN2 (e.g., P525 and V538 mutants) produced spherical droplets of similar size as WT. Mutants that exhibited significantly enhanced turbidity (P497W, P497L, P506W, P506L) also formed amorphous droplets (Figures 1C and 3A). Microscopy also confirmed the existence of aggregates as observed in the turbidity assays for P497Q (P506Q aggregates were observed at temperatures higher than 37 °C during the turbidity assays and therefore were not seen under the microscope). Surprisingly, acidic substitution E, which showed little or no turbidity at the condition tested, appeared to form small aggregate-like species at all five positions at our experimental conditions. Over time, these aggregate-like species sometimes morphed into droplets as observed for V538E (Figure 3A). Consistent with our hypothesis, mutations at spacer positions 525 and 538 (except V525R, P525E, and V538E) had minimal effects on the morphology of the droplets, while mutations at sticker positions 497, 506, and 564 elicited different morphologies ranging from round like WTlike to amorphous droplets and/or aggregates.

To describe the effects of amino acid substitutions on the properties of the dense phase quantitatively, we analyzed droplet fusion kinetics. We noticed that, for many substitutions, two fusing droplets relaxed into spherical shapes within seconds, while for other substitutions, spherical shapes were not achieved within a 3 min experimental window (Figure 3B). Since the sphericity of droplets stems from surface tension, the rates of droplet fusion report on droplet viscosity and surface tension.³¹ To assess the liquidity of mutant UBQLN2 droplets, we measured the time it took for two fusing droplets to return to a spherical shape (or round in two dimensions). We extracted relaxation times from droplet fusion measurements for seven amino acid substitutions at the sticker and spacer positions, 506 and 538, respectively, of protein samples that had been incubated in phase-separating conditions for 10 min (Figure 3B,C). Remarkably, droplets for

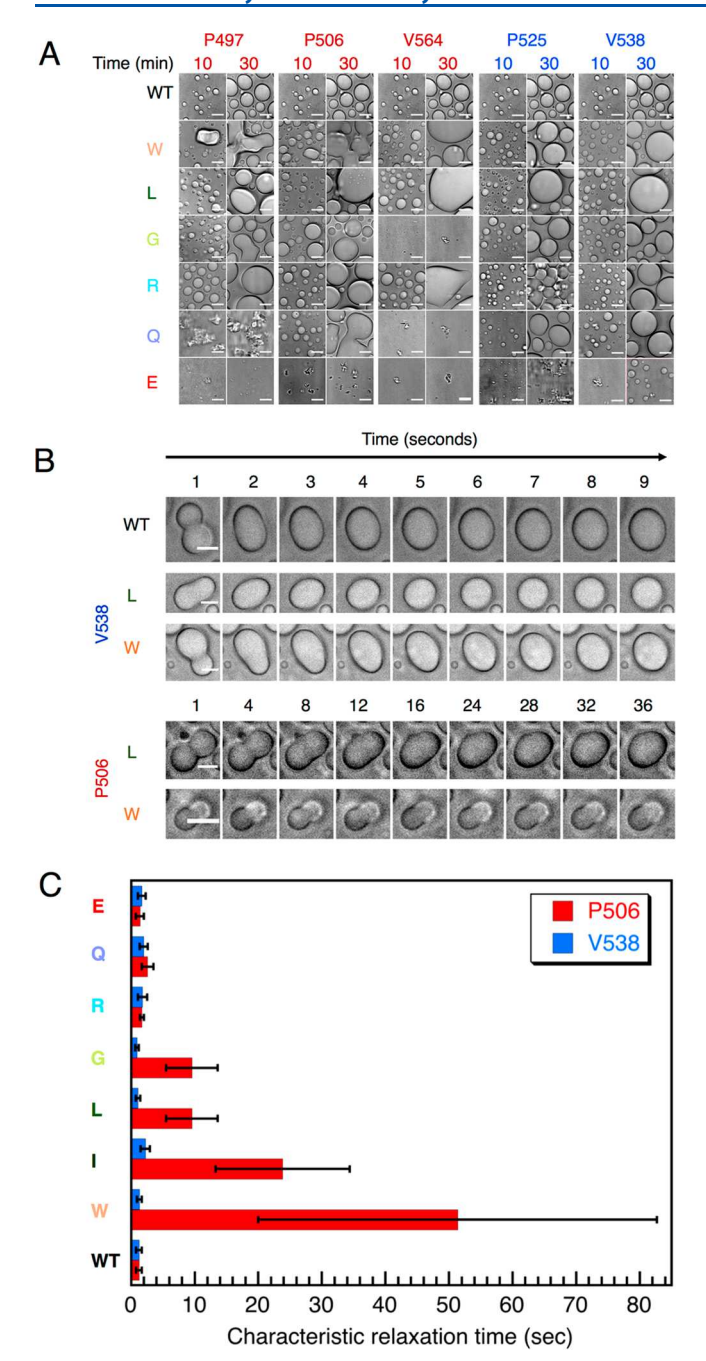


Figure 3. Amino acid substitutions in the sticker, but not spacer, regions affect droplet properties. (A) Light microscopy of different UBQLN2 mutants over 10 and 30 min at 37 °C using 100 μ M protein at sticker (P497, P506, V564) and spacer (P525, V538) positions. Scale bar = 5 μ m. (B) Snapshots of droplet fusion over a nine second window (for WT and V538L and V538W) and a 36 s window (for P506L and P506W), indicating differences in droplet fusion kinetics between substitutions at a sticker position (P506) and a spacer position (V538). Droplets were imaged 10 min after incubating 100 μ M protein (except for P506W (25 μ M), P506E and V538E (300 μ M)) at 37 °C in buffer containing 20 mM NaPhosphate and 200 mM NaCl (pH 6.8). Scale bar = 2 μ m. (C) Average characteristic relaxation times for WT and mutant droplet fusion. Error bars represent the standard deviation over eight droplets.

V538 mutants fused quickly and with similar relaxation times as that for WT UBQLN2, despite the markedly different types of amino acid substitutions tested. These observations are fully

consistent with the spacer characteristics expected for position 538, in that spacer amino acid substitutions minimally perturbed phase separation properties. In contrast, the type of amino acid substitution at sticker position 506 had a substantial impact on the rate of droplet relaxation. Bulky aromatic and hydrophobic substitutions resulted in significantly slowed droplet relaxation events, but not for polar and ionizable substitutions. These data suggest that hydrophobic and aromatic amino acids promote UBQLN2 intermolecular interactions that increase viscoelasticity of UBQLN2 droplets as well as drive UBQLN2 phase separation (see below).

Hydrophobic and Aromatic Sticker Substitutions Increase UBQLN2 Oligomerization. As UBQLN2 oligomerization is a prerequisite for phase separation, ²⁵ we probed UBQLN2 self-association propensity using SEC under nonphase separating conditions (i.e., 20 mM NaPhosphate without added NaCl). We previously demonstrated that WT UBQLN2 is monomeric at low protein concentrations (up to ~100 μ M) but forms higher-order oligomers at higher concentrations (~500 μ M). ²⁵ Indeed, SEC peak elution volumes for WT decreased as protein concentration increased between 10 and 500 μ M, as expected for UBQLN2 oligomerization. Therefore, we subjected representative mutants at each position to size exclusion chromatography using three protein concentrations (10, 100, 500 μ M).

All of the mutants studied exhibited concentration-dependent oligomerization; increasing protein concentrations led to a decrease in elution volume (Figure 4). Strikingly, almost all of the spacer mutants (P525 and V538) exhibited a concentration dependence that followed the pattern of WT UBQLN2. The only exception was P525E, where a small population of large particles eluted near the void volume (~9 mL). Of all the E mutants, P525E showed the most aggregates by microscopy (Figure 3A). Among the sticker mutants, four oligomerized substantially more than WT: P497W, P497L, P506W, and P506L. Sedimentation velocity analytical ultracentrifugation experiments showed that hydrophobic mutations T487I and P497L also produced high-order oligomers. 43 V564W and V564L oligomerized slightly more than WT but not to a significant extent, since the wild-type amino acid is valine, which is already hydrophobic. These data suggest that aromatic and hydrophobic substitutions promote UBQLN2 selfassociation and thus drive LLPS at lower protein concentrations than WT (Figure 2) and enhance the viscoelasticity of droplets (Figure 3).

DISCUSSION

How amino acid substitutions alter thermoresponsive phase transition behavior of proteins is critical to elucidating the driving forces of phase separation. Here, we demonstrated that both LCST and UCST phase transition behaviors of UBQLN2 can be differentially tuned by single amino acid substitutions. The observations herein provide evidence that the stickers and spacers framework is useful to predicting the positions in a given amino acid sequence that drive phase separation behavior. Regardless of amino acid type, substitutions at sticker but not spacer positions elicited major changes to the overall shape and characteristics of the phase diagram (Figures 2 and 5).

Our original hypothesis considered the stickers of UBQLN2 to be residues that exhibited large concentration-dependent changes in amide chemical shifts obtained by NMR spectroscopy.²⁵ In the stickers and spacers framework, the number of

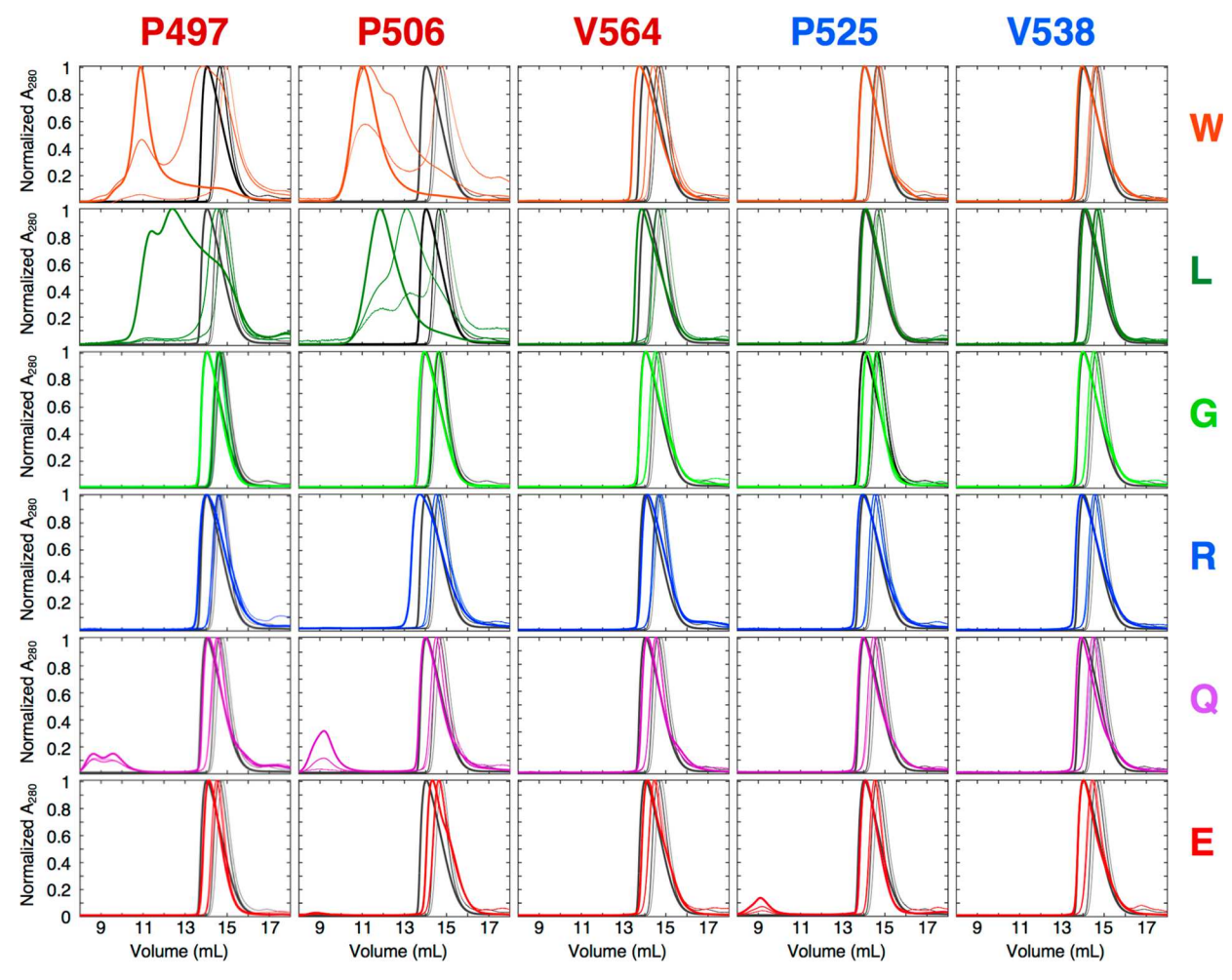


Figure 4. Oligomerization propensities of different UBQLN2 mutants. Representative SEC profiles of UBQLN2 mutants at $10 \,\mu\text{M}$ (thinnest line), $100 \,\mu\text{M}$ (medium-thick), and $500 \,\mu\text{M}$ (thickest) protein concentrations. For each mutant, WT SEC curves were plotted in gray for visual comparison.

stickers and their "stickiness" control the saturation concentrations (c_s) and the coexistence curve for LLPS, whereas spacer residues weakly modulate these parameters. These expectations are completely in line with our observations on amino acid substitutions at the three stickers (P497, P506, and V564) and two spacers (P525, V538) (Figure 1C,B). Strikingly, not only did single amino acid substitutions alone substantially shift c_s values but the effects of these substitutions followed particular trends to create a rich molecular code that governs UBQLN2 LLPS.

Self-association and LLPS of UBQLN2 are mediated by hydrophobicity involving either aliphatic or aromatic residues (Figure 2, Figure 4), in line with the hydrophobic composition of the amino acid sequence (Figure 1B). At position 506, decreased $c_{\rm s}$ values for the LCST phase transition correlated with increased hydrophobicity of amino acid substitution (Figure S5). Indeed, while we did not obtain phase diagrams for P497 mutants, the LCST transition temperatures for aromatic and hydrophobic substitutions at P497 followed the same trend as that at P506 (Figure 1C). LCST phase transitions require hydrophobicity. ^{22,25,32} UBQLN2 also has high proline and glycine content (Figure 1B), which is a frequent component of proteins that undergo LCST phase transitions, such as Pab1, tropoelastins, and the spindle-associated BuGZ protein. ^{14,15,33}

UBQLN2 exhibits a closed-loop phase diagram with both LCST and UCST phase transitions, such that the protein solution is well-mixed either above the UCST or below the LCST (Figure 2A). The thermodynamics of the underlying phase transitions can be explained by the entropic and enthalpic forces experienced by nonpolar particles in water as a function of temperature.³⁴ At low temperature, solubility of hydrophobic particles is high, partially due to water structuring around the hydrophobic groups. As temperature increases, the entropic cost to organize water also increases to a point at which solvent molecules are released from surrounding hydrophobic side chains, promoting demixing (phase separation) to minimize the free energy of the system. In polymer solutions, dehydration of hydrophobic groups is accompanied by attractive polymer-polymer interactions that also contribute to demixing.³⁵ As temperature increases further, entropy also increases promoting a UCST transition where homogeneous mixing of the polymer solution occurs. A decrease in polymer-polymer and solvent-solvent interactions also promotes mixing.³⁶ This UCST transition is not always observed, as biopolymers generally denature at high temperatures, but UBQLN2 450-624 remains well-behaved up to 60 °C.43

As illustrated in Figure 1B, more than 25% of UBQLN2 450-624 contains polar residues (Q, N, S, T). Therefore, the

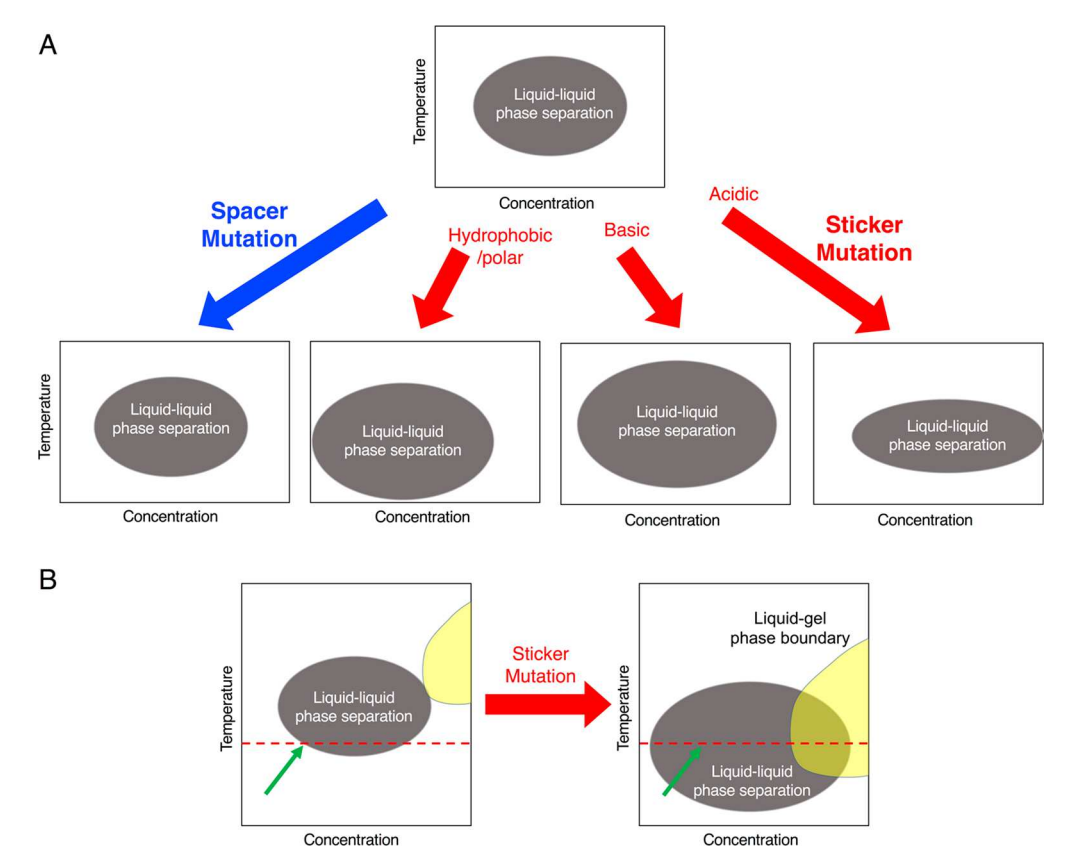


Figure 5. Illustration of effects of UBQLN2 sticker and spacer substitutions on temperature—concentration phase diagrams. (A) Effects of spacer and different types of sticker substitutions on the shape of the phase diagram. Amino acid substitutions in sticker regions move the location and shape of the phase boundaries. However, high concentration arms are hypothetical and for illustration purposes only. We hypothesize that the high concentration arms of some of the sticker mutants also move as we observed changes to the material properties of the dense phase. (B) Effects of mutations on phase diagrams and viscoelasticity. Gray and yellow shapes represent regions where the dense phase is liquid-like and gel/aggregate-like, respectively. (left) Green arrow represents a condition where dense phase is solid-like (i.e., gel-like consistency).

driving forces underlying UBQLN2 phase separation are likely due to a combination of the hydrophobic effect and polar interactions. Of note, polymers rich in polar residues (N, Q) undergo a collapse transition reminiscent of the intrachain collapse in hydrophobic biopolymers, even though the underlying forces for polar collapse likely include other interactions such as intrachain hydrogen bonding and amide—solvent interactions. ^{28,37} Interestingly, the $c_{\rm s}$ values for the LCST transition correlated well with the hydrophobicity of the amino acid substitution at P506 when all nonionizable residues were considered (Figure S5B). Polar substitutions also promoted aggregation (Figure S2E).

The polar groups in UBQLN2 likely modulate the UCST transition, as favorable polymer—polymer interactions among polar and/or ionizable tracts in intrinsically disordered proteins (IDPs) such as FUS and hnRNPA1 are considered drivers of UCST transitions in biopolymers. An increase and decrease in the UCST part of coexistence curves correspond to stronger and weaker polymer—polymer interactions, respectively. Complicating matters, hydrophobic groups also modulate UCST, and the effects of hydrophobic amino acid substitutions on the UCST transitions in UBQLN2 are certainly complex. At P506, increased hydrophobicity moderately tracks with decreased cloud-point temperatures for the UCST transition (Figure S5A). Our observations are opposite of what was seen in designed IDP polymers, for which UCST cloud points increased with increasing hydrophobicity. Interestingly, our

turbidity data profile for hydrophobic substitutions at P497 are in better agreement with Quiroz et al.³⁸ We must acknowledge that prolines are structure-disrupting amino acids. In addition, peptide bonds preceding prolines can isomerize between *cis* and *trans* conformations. Therefore, the differences in observed turbidity profiles for proline substitutions at different positions could be partially explained by changes to backbone conformation and flexibility. These observations emphasize the heterogeneity of the phase transition behavior for the same type of amino acid substitution even among the sticker positions.

Remarkably, Asp and Glu mutations at any of the five tested positions in UBQLN2 reduced phase separation and significantly compressed the phase-separating regime in the UBQLN2 phase diagram (Figure 2). Importantly, these acidic mutations are also phosphomimetic substitutions. These data highlight the potential impact of post-translational modifications such as phosphorylation on modulating phase separation behavior. However, the effect is likely very dependent on the electrostatics of the protein system involved. 8,39

Material properties of the dense phase are also modified by amino acid substitutions. The liquid—liquid phase diagram therefore includes liquid-gel phase boundaries as schematized in Figure 5.6 Indeed, the stickers and spacers framework is one formalism that quantitatively addresses gelation. We observed that hydrophobic and aromatic amino acid substitutions only in sticker position P506 showed significantly

slowed droplet fusion kinetics (Figure 3), and those same mutants exhibited increased oligomerization propensity (Figure 4). At least in the UBQLN2 system, material properties of the dense phase appear linked to the propensity for UBQLN2 to oligomerize. We also noted that mutations that increased the propensity of oligomerization promoted UBQLN2 LLPS and led to slowed droplet fusion kinetics. However, this is not always the case, as spacer mutations significantly slowed droplet fusion kinetics in the FUS family of proteins, and physicochemical properties of spacers in multidomain proteins modulate the liquid—liquid and liquid—gel phase boundaries.

In summary, our work here provides a rich data set to be used as a benchmark for analytical and computational models of phase separation. While mean-field theories such as Flory—Huggins approximate phase separation behavior for several systems, ^{18,41} sequence-dependent frameworks will be essential to capture the nuances of phase-separating systems such as UBQLN2. ⁴² The stickers and spacers framework has already been used to successfully examine the underlying forces of phase separation in the FET family of RNA-binding proteins. ⁸ Unraveling the complexities of solvent—solvent, polymer—polymer, and polymer—solvent interactions will establish the molecular code of phase-separating systems.

CONCLUSIONS

In this work, we put forth UBQLN2 450-624 as a model system to study the physicochemical molecular determinants of phase separation. We employed a battery of spectrophotometric, microscopy, and size exclusion chromatography experiments to systematically elucidate how amino acid substitutions at different positions in the protein sequence modulate phase separation. Experimental phase diagrams revealed that we can describe UBQLN2 as an associative polymer with stickers and spacers that drive and modulate phase separation behavior. Single amino-acid substitution can substantially shift coexistence curves in a residue typedependent manner. It is our expectation that our experimental data can be used to rigorously design and benchmark analytical models and molecular simulations of phase separation. This work can be used to elucidate effects of disease-linked mutations in phase-separating systems as well as to design thermoresponsive biopolymers.

ASSOCIATED CONTENT

S Supporting Information

The Supporting Information is available free of charge on the ACS Publications website at DOI: 10.1021/acs.jpcb.9b01024.

Figures of UBQLN2 sequence information, representative gels, and mass spectrometry of UBQLN2 mutants, reproducibility of turbidity assays and size exclusion chromatography experiments, and correlations between saturation concentrations and hydrophobicity (PDF)

AUTHOR INFORMATION

Corresponding Author

*E-mail: cacastan@syr.edu.

ORCID

Carlos A. Castañeda: 0000-0001-9634-0867

Author Contributions

The manuscript was written through contributions of all authors. All authors have given approval to the final version of the manuscript.

Notes

The authors declare no competing financial interest.

Biography



Carlos A. Castañeda received his Ph.D. from the Program in Molecular Biophysics at Johns Hopkins University working with Dr. Bertrand Garcia-Moreno on using NMR spectroscopy and electrostatics calculations to measure and calculate the pK_a values of ionizable groups in proteins. As an NSF postdoctoral fellow, he worked with David Fushman at the University of Maryland-College Park on studying the structure and function of all polyubiquitin chain types using NMR spectroscopy, small angle scattering, and computational modeling. In his independent lab at Syracuse University, where he is an assistant professor of Biology and Chemistry, Carlos focuses on elucidating the role of protein quality control mechanisms in neurological disorders, such as amyotrophic lateral sclerosis (ALS). Since discovering that UBQLN2 undergoes liquid-liquid phase separation in vitro and in vivo, his lab has focused on determining the molecular basis for phase separation in ubiquilins and other proteins using a combination of experimental and computational tools. For this work, Carlos has received two grants from the ALS Association and an NSF CAREER award in 2018.

ACKNOWLEDGMENTS

This work was supported by ALS Association Grant No. 18-IIP-400 and the National Science Foundation (CAREER Award No. 1750462) to C.A.C. We thank A. Sorrano and participants at the Gibbs Conference on Biothermodynamics for useful discussions. The Shimadzu 8040 mass spectrometer was partially supported by a Shimadzu equipment grant to C.A.C.

REFERENCES

- (1) Brangwynne, C. P.; Eckmann, C. R.; Courson, D. S.; Rybarska, A.; Hoege, C.; Gharakhani, J.; Jülicher, F.; Hyman, A. A. Germline P Granules Are Liquid Droplets That Localize by Controlled Dissolution/Condensation. *Science* **2009**, *324*, 1729–1732.
- (2) Hyman, A. A.; Weber, C. A.; Jülicher, F. Liquid-Liquid Phase Separation in Biology. *Annu. Rev. Cell Dev. Biol.* **2014**, *30*, 39–58.
- (3) Banani, S. F.; Rice, A. M.; Peeples, W. B.; Lin, Y.; Jain, S.; Parker, R.; Rosen, M. K. Compositional Control of Phase-Separated Cellular Bodies. *Cell* **2016**, *166*, *651*–*663*.
- (4) Li, P.; Banjade, S.; Cheng, H.-C.; Kim, S.; Chen, B.; Guo, L.; Llaguno, M.; Hollingsworth, J. V.; King, D. S.; Banani, S. F.; et al.

- Phase Transitions in the Assembly of Multi-Valent Signaling Proteins. *Nature* **2012**, *483*, 336–340.
- (5) Lin, Y.; Protter, D. S. W.; Rosen, M. K.; Parker, R. Formation and Maturation of Phase-Separated Liquid Droplets by RNA-Binding Proteins. *Mol. Cell* **2015**, *60*, 208–219.
- (6) Lin, Y.; Currie, S. L.; Rosen, M. K. Intrinsically Disordered Sequences Enable Modulation of Protein Phase Separation through Distributed Tyrosine Motifs. *J. Biol. Chem.* **2017**, 292, 19110–19120.
- (7) Pak, C. W.; Kosno, M.; Holehouse, A. S.; Padrick, S. B.; Mittal, A.; Ali, R.; Yunus, A. A.; Liu, D. R.; Pappu, R. V.; Rosen, M. K. Sequence Determinants of Intracellular Phase Separation by Complex Coacervation of a Disordered Protein. *Mol. Cell* **2016**, *63*, 72–85.
- (8) Wang, J.; Choi, J.-M.; Holehouse, A. S.; Lee, H. O.; Zhang, X.; Jahnel, M.; Maharana, S.; Lemaitre, R.; Pozniakovsky, A.; Drechsel, D.; et al. A Molecular Grammar Governing the Driving Forces for Phase Separation of Prion-like RNA Binding Proteins. *Cell* **2018**, *174*, 688–699.
- (9) Molliex, A.; Temirov, J.; Lee, J.; Coughlin, M.; Kanagaraj, A. P.; Kim, H. J.; Mittag, T.; Taylor, J. P. Phase Separation by Low Complexity Domains Promotes Stress Granule Assembly and Drives Pathological Fibrillization. *Cell* **2015**, *163*, 123–133.
- (10) Patel, A.; Lee, H. O.; Jawerth, L.; Maharana, S.; Jahnel, M.; Hein, M. Y.; Stoynov, S.; Mahamid, J.; Saha, S.; Franzmann, T. M.; et al. A Liquid-to-Solid Phase Transition of the ALS Protein FUS Accelerated by Disease Mutation. *Cell* **2015**, *162*, 1066–1077.
- (11) Harmon, T. S.; Holehouse, A. S.; Rosen, M. K.; Pappu, R. V. Intrinsically Disordered Linkers Determine the Interplay between Phase Separation and Gelation in Multivalent Proteins. *eLife* **2017**, *6*, No. e30294.
- (12) Rubinstein, M.; Dobrynin, A. V. Solutions of Associative Polymers. *Trends Polym. Sci.* **1997**, *5*, 181–186.
- (13) Semenov, A. N.; Rubinstein, M. Thermoreversible Gelation in Solutions of Associative Polymers. *Macromolecules* **1998**, *31*, 1373–1385
- (14) Riback, J. A.; Katanski, C. D.; Kear-Scott, J. L.; Pilipenko, E. V.; Rojek, A. E.; Sosnick, T. R.; Drummond, D. A. Stress-Triggered Phase Separation Is an Adaptive, Evolutionarily Tuned Response. *Cell* **2017**, *168*, 1028–1040.
- (15) Yeo, G. C.; Keeley, F. W.; Weiss, A. S. Coacervation of Tropoelastin. *Adv. Colloid Interface Sci.* **2011**, *167*, 94–103.
- (16) Zai-Rose, V.; West, S. J.; Kramer, W. H.; Bishop, G. R.; Lewis, E. A.; Correia, J. J. Effects of Doxorubicin on the Liquid-Liquid Phase Change Properties of Elastin-Like Polypeptides. *Biophys. J.* **2018**, *115*, 1431–1444.
- (17) Li, H.-R.; Chiang, W.-C.; Chou, P.-C.; Wang, W.-J.; Huang, J. TAR DNA-Binding Protein 43 (TDP-43) Liquid–Liquid Phase Separation Is Mediated by Just a Few Aromatic Residues. *J. Biol. Chem.* **2018**, 293, 6090–6098.
- (18) Nott, T. J.; Petsalaki, E.; Farber, P.; Jervis, D.; Fussner, E.; Plochowietz, A.; Craggs, T. D.; Bazett-Jones, D. P.; Pawson, T.; Forman-Kay, J. D.; et al. Phase Transition of a Disordered Nuage Protein Generates Environmentally Responsive Membraneless Organelles. *Mol. Cell* **2015**, *57*, 936–947.
- (19) Vernon, R. M.; Chong, P. A.; Tsang, B.; Kim, T. H.; Bah, A.; Farber, P.; Lin, H.; Forman-Kay, J. D. Pi-Pi Contacts Are an Overlooked Protein Feature Relevant to Phase Separation. *eLife* **2018**, 7. No. e31486.
- (20) Posey, A. E.; Holehouse, A. S.; Pappu, R. V. Chapter One Phase Separation of Intrinsically Disordered Proteins. *Methods Enzymol.* **2018**, *611*, 1–30.
- (21) Rubinstein, M.; Colby, R. H. Polymer Physics; Oxford University Press: Oxford, UK, 2003.
- (22) Ruff, K. M.; Roberts, S.; Chilkoti, A.; Pappu, R. V. Advances in Understanding Stimulus-Responsive Phase Behavior of Intrinsically Disordered Protein Polymers. *J. Mol. Biol.* **2018**, *430*, 4619–4635.
- (23) Alberti, S.; Gladfelter, A.; Mittag, T. Considerations and Challenges in Studying Liquid-Liquid Phase Separation and Biomolecular Condensates. *Cell* **2019**, *176*, 419–434.

- (24) Dzuricky, M.; Roberts, S.; Chilkoti, A. Convergence of Artificial Protein Polymers and Intrinsically Disordered Proteins. *Biochemistry* **2018**, *57*, 2405–2414.
- (25) Dao, T. P.; Kolaitis, R.-M.; Kim, H. J.; O'Donovan, K.; Martyniak, B.; Colicino, E.; Hehnly, H.; Taylor, J. P.; Castañeda, C. A. Ubiquitin Modulates Liquid-Liquid Phase Separation of UBQLN2 via Disruption of Multivalent Interactions. *Mol. Cell* **2018**, *69*, 965–978.
- (26) Schindelin, J.; Arganda-Carreras, I.; Frise, E.; Kaynig, V.; Longair, M.; Pietzsch, T.; Preibisch, S.; Rueden, C.; Saalfeld, S.; Schmid, B.; et al. Fiji: An Open-Source Platform for Biological-Image Analysis. *Nat. Methods* **2012**, *9*, 676–682.
- (27) Mutterer, J.; Zinck, E. Quick-and-Clean Article Figures with Figure J. Microsc. 2013, 252 (1), 89–91.
- (28) Holehouse, A. S.; Pappu, R. V. Collapse Transitions of Proteins and the Interplay Among Backbone, Sidechain, and Solvent Interactions. *Annu. Rev. Biophys.* **2018**, *47*, 19–39.
- (29) Urry, D. W.; Gowda, D. C.; Parker, T. M.; Luan, C.-H.; Reid, M. C.; Harris, C. M.; Pattanaik, A.; Harris, R. D. Hydrophobicity Scale for Proteins Based on Inverse Temperature Transitions. *Biopolymers* 1992, 32, 1243–1250.
- (30) Osváth, Z.; Iván, B. The Dependence of the Cloud Point, Clearing Point, and Hysteresis of Poly(N-Isopropylacrylamide) on Experimental Conditions: The Need for Standardization of Thermoresponsive Transition Determinations. *Macromol. Chem. Phys.* **2017**, 218, 1600470.
- (31) Feric, M.; Vaidya, N.; Harmon, T. S.; Mitrea, D. M.; Zhu, L.; Richardson, T. M.; Kriwacki, R. W.; Pappu, R. V.; Brangwynne, C. P. Coexisting Liquid Phases Underlie Nucleolar Sub-Compartments. *Cell* **2016**, *165*, 1686–1697.
- (32) Martin, E. W.; Mittag, T. Relationship of Sequence and Phase Separation in Protein Low-Complexity Regions. *Biochemistry* **2018**, 57, 2478–2487.
- (33) Jiang, H.; Wang, S.; Huang, Y.; He, X.; Cui, H.; Zhu, X.; Zheng, Y. Phase Transition of Spindle-Associated Protein Regulate Spindle Apparatus Assembly. *Cell* **2015**, *163*, 108–122.
- (34) Moelbert, S.; Normand, B.; De Los Rios, P. Solvent-Induced Micelle Formation in a Hydrophobic Interaction Model. *Phys. Rev. E. Stat. Nonlin. Soft Matter Phys.* **2004**, *69*, 061924.
- (35) Matsarskaia, O.; Braun, M. K.; Roosen-Runge, F.; Wolf, M.; Zhang, F.; Roth, R.; Schreiber, F. Cation-Induced Hydration Effects Cause Lower Critical Solution Temperature Behavior in Protein Solutions. *J. Phys. Chem. B* **2016**, *120*, 7731–7736.
- (36) Falahati, H.; Haji-Akbari, A. Thermodynamically Driven Assemblies and Liquid–Liquid Phase Separations in Biology. *Soft Matter* **2019**, *15*, 1135–1154.
- (37) Wuttke, R.; Hofmann, H.; Nettels, D.; Borgia, M. B.; Mittal, J.; Best, R. B.; Schuler, B. Temperature-Dependent Solvation Modulates the Dimensions of Disordered Proteins. *Proc. Natl. Acad. Sci. U. S. A.* **2014**, *111*, 5213–5218.
- (38) Quiroz, F. G.; Chilkoti, A. Sequence Heuristics to Encode Phase Behaviour in Intrinsically Disordered Protein Polymers. *Nat. Mater.* **2015**, *14*, 1164–1171.
- (39) Monahan, Z.; Ryan, V. H.; Janke, A. M.; Burke, K. A.; Rhoads, S. N.; Zerze, G. H.; O'Meally, R.; Dignon, G. L.; Conicella, A. E.; Zheng, W.; et al. Phosphorylation of the FUS Low-complexity Domain Disrupts Phase Separation, Aggregation, and Toxicity. *EMBO J.* 2017, 36, 2951–2967.
- (40) Kato, M.; Han, T. W.; Xie, S.; Shi, K.; Du, X.; Wu, L. C.; Mirzaei, H.; Goldsmith, E. J.; Longgood, J.; Pei, J.; et al. Cell-Free Formation of RNA Granules: Low Complexity Sequence Domains Form Dynamic Fibers within Hydrogels. *Cell* **2012**, *149*, 753–767.
- (41) Brady, J. P.; Farber, P. J.; Sekhar, A.; Lin, Y.-H.; Huang, R.; Bah, A.; Nott, T. J.; Chan, H. S.; Baldwin, A. J.; Forman-Kay, J. D.; et al. Structural and Hydrodynamic Properties of an Intrinsically Disordered Region of a Germ Cell-Specific Protein on Phase Separation. *Proc. Natl. Acad. Sci. U. S. A.* **2017**, *114*, E8194—E8203.
- (42) Lin, Y.-H.; Forman-Kay, J. D.; Chan, H. S. Theories for Sequence-Dependent Phase Behaviors of Biomolecular Condensates. *Biochemistry* **2018**, *57*, 2499–2508.

Article

(43) Dao, T. P.; Martyniak, B.; Canning, A. J.; Lei, Y.; Colicino, E. G.; Cosgrove, M. S.; Hehnly, H.; Castañeda, C. A. ALS-linked mutations affect UBQLN2 oligomerization and phase separation in a position- and amino acid-dependent manner. *Structure* **2019**, DOI: 10.1016/j.str.2019.03.012.